Efficient Diagnosis of Radiotelescopes Misalignments

Amedeo Capozzoli
Angelo Liseno
Claudio Curcio
Salvatore Savarese
Dipartimento di Ingegneria Elettrica e Tecnologie dell'Informazione (DIETI)
Università degli Studi di Napoli Federico II
via Claudio 21, 80125 Napoli (Italy)

Pietro Schipani
INAF - Istituto Nazionale di Astrofisica
Salita Moiariello 16, 80131 Napoli (Italy)

***Abstract*— An innovative method for the diagnosis of large reflector antennas from far field data in radio astronomical application is presented, which is based on the optimization of the number and the location of the far field sampling points required to retrieve the antenna status in terms of feed misalignments. In these applications a continuous monitoring of the Antenna Under Test (AUT), and its subsequent reassessment, is necessary to guarantee the optimal performances of the radiotelescope. The goal of the proposed method is to reduce the measurement time length in order to minimize the effects of time variations of the measurement setup, as well as the problems associated to the complex tracking of the source required by a prolonged acquisition, which can be detrimental to the effectiveness of the diagnosis. Furthermore, a short measurement process helps to shorten the idle time forced by the maintenance activity.**

The diagnosis problem is cast as a linear inverse one. The field radiated by the AUT is described by the aperture field method. The effects of the feed misalignments are modeled in terms of an aberration function, properly expanded by a set of basis functions determined using the Principal Component Analysis in order to retain a linear relationship between the unknown parameters defining the antenna status and the far field pattern, assumed measured in amplitude and phase. The number and the position of the samples is then found by a Singular Values behavior optimization.

I. INTRODUCTION

In order to get the best performances of large reflector antennas for radio astronomical applications, a continuous monitoring and the reassessment of the Antenna Under Test (AUT) is necessary [1-3]. In particular, getting the maximum gain and the correct pointing angle require the suppression of the deviations of the reflecting surfaces [4] from their nominal profiles, and the correct alignment of reflectors and feeding structure.

Among the different approaches adopted in the last decades, the electromagnetic monitoring appears today one of the most appealing. The electromagnetic monitoring allows in-situ measurements, with little direct human intervention, and employs a relatively simple setup. The approach retrieves the distortions and the misalignments from amplitude and phase, or only amplitude, measurements of Far-Field Pattern (FFP) of the AUT. The FFP is typically measured with the AUT in the receiving mode and by adopting a natural radio star or a satellite beacon as the signal source [1,2]. To acquire the FFP in amplitude and phase, a second antenna must be considered to generate a reference signal, allowing the holographic approach [4]. A simpler approach is possible by measuring the amplitude of the FFP only [5-7]. This alternative does not require any reference antenna and demands a simpler measurement setup. Obviously, additional information about the AUT or a second set of measurements is required to restore the missed information.

In both cases, a very large number of field samples is required to get the complete information about the AUT, and the subsequent measurements may span over several hours. To limit problems related to variation of measurement parameters, e.g. due to thermal stress of structures, acquisitions no longer than 12 hours are required [1]. In addition to a complete diagnosis of the AUT, it is necessary to dispose of a fast procedure able to quick provide information with a lower resolution, in order to assess the correct alignment of the feed and the sub reflector (if present). To this end a proper strategy turns relevant, to reduce as much as possible the time length of the measurements process, and to increase the robustness of the inversion against noise and reduced dynamical ranges. Indeed it is expected that the number of parameters to be retrieved on the AUT significantly influences the acquisition strategy.

Aim of the paper is to present an approach to define the number and the distribution of the FFP samples according to the desired monitoring resolution. The approach recasts the diagnosis in terms of a linear inverse problem, and the goal is achieved thanks to a Singular Values Behavior (SVB) optimization of the relevant operator mapping the parameters defining the misalignments to the FFP.

The paper is organized as follows. Section 2 introduce the mathematical model of the problem, in Section 3 the solution algorithm is presented, while Section 4 shows and discusses some numerical results limited to the case of a lateral feed displacement. The performances are compared to those of a standard approach based on a standard sampling acquisition scheme.

II. STATEMENT OF THE PROBLEM

Let us consider as AUT a reflector antenna, whose aperture A lies in the z=0 plane of the (Oxyz) reference system schematically depicted in Figure 1. . The Aperture Field (AF) method is employed to describe the radiation mechanism of the AUT. In particular, for the sake of simplicity and without any loss of generality, we consider a scalar problem, assuming that the AF, say $\underline{E_a}$, is linearly polarized along the x-axis: $\underline{E_a} = E_a \underline{i}_x$.

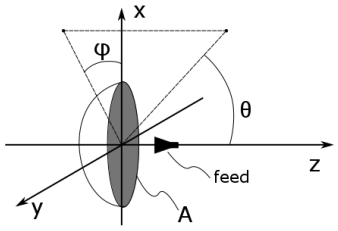

Figure 1. Geometry of the problem.

Monochromatic signals will be considered, and the time dependence $exp(j\omega t)$ assumed and dropped.

The relationship between the x-component of the FFP, say F, and E_a is easily expressed, apart from inessential constants, via the well-known Fourier Transform relationship [8]:

$$F = \cos\theta \iint_A dx\, dy\, E_a exp\big(j\beta(ux + vy)\big) = \boldsymbol{\mathcal{T}}\,[E_a] \quad (1)$$

where:

- $u = \sin\theta\cos\varphi$ and $v = \sin\theta\sin\varphi$ are the cosine directors
- $\beta = 2\pi/\lambda$, λ being the wavelength;
- $\boldsymbol{\mathcal{T}}$ is the operator mapping the AF on the FFP.

Misalignments and distortions of the reflecting surfaces alter E_a from its nominal value. Accordingly, monitoring the AUT amounts at determining first E_a from the FFP, and then inverting the desired configuration parameters.

In the paper we focus our attention on the misalignment of the feeding system. Assuming that its displacement keeps small, we can assume that the deviation from the nominal configuration affects only the phase distribution of E_a. We can then introduce a real valued aberration function $\Phi(x, y; p_1, \dots, p_N)$ representing the phase perturbation as a function of N parameters $p_1, \dots, p_N$ describing the status of the AUT to be retrieved. With these assumptions, the AF can be written as:

$$E_a(x, y) = E_{a0}(x, y) exp\big(j\Phi(x, y; p_1, \dots, p_N)\big) \quad (2)$$

where E_{a0} is the nominal AF, corresponding to the undistorted configuration.

The diagnosis problem consists of determining Φ from the FFP, and then the parameters $p_1, \dots, p_N$ describing its status. Accordingly, the solution of an inverse problem is required.

III. THE SOLUTION ALGORITHM

To recast the inverse problem as a linear one, we consider a proper representation of $exp\big(j\Phi(x, y; p_1, \dots, p_N)\big)$, noting that it defines a manifold $\mathcal{M}$ in the space of functions with two variables (x, y), as long as $(p_1, \dots, p_N)$ are varied in the intervals defining the acceptable indeterminacies for the parameters defining the AUT status. We can then introduce the set of basis functions $\{\psi_1, \dots, \psi_K\}$ defining the smallest subspace containing $\mathcal{M}$. Accordingly:

$$exp\big(\phi(x, y; p_1, \dots, p_N)\big) = \sum_{k=1}^{K} c_k(p_1, \dots, p_N)\psi_k(x, y) \quad (3)$$

The set of basis functions $\{\psi_1, \dots, \psi_K\}$ can been found thanks to a Principal Component Analysis (PCA).

Concerning the FFP, it is assumed sampled at S points (u_s, v_s). Equation (1) can be then written in matrix form as:

$$\underline{F} = \underline{\underline{T}}\,\underline{C} \quad (4)$$

where $\underline{F}$ and $\underline{C}$ are the S-dimensional vector containing the field samples and the K-dimensional vector of the expansion coefficients, respectively. The entries of the matrix $\underline{\underline{T}}$ are given by:

$$T_{sk} = \langle \boldsymbol{\mathcal{T}}\,[E_{a0}\psi_k], \delta(u - u_s)\delta(v - v_s)\rangle \quad (5)$$

δ being the Dirac distribution.

Retrieving the AUT status amounts at finding the coefficients c_k, and then the parameters $p_1, \dots, p_N$, from $\underline{F}(u_s, v_s)$. As a consequence, the inversion of the linear algebraic system in Equation (4) is required. Obviously, such a system can suffer from the ill-conditioning, with detrimental effects on the accuracy of the reconstruction and on the robustness against noise.

$\underline{\underline{T}}$ depends on the samples distribution in the (u, v) plane. We consider a plane-polar arrangement of (u_s, v_s), so that they are located on M rings with radii ρ_m, and therein uniformly spaced with sampling step $\Delta\chi_m$ [9], as shown in Figure 2. .

Before inverting $\underline{\underline{T}}$, the most convenient matrix must be picked up, by optimizing its SVB as a function of M, ρ_m and $\Delta\chi_m$.

The optimization of the SVB of $\underline{\underline{T}}$ can be obtained by maximizing the functional [10]:

$$\Psi\left(\underline{\rho}, \underline{\Delta\chi}\right) = \sum_r \frac{\sigma_r\left(\underline{\rho}, \underline{\Delta\chi}\right)}{\sigma_1\left(\underline{\rho}, \underline{\Delta\chi}\right)} \quad (6)$$

where $\underline{\rho}$ and $\underline{\Delta\chi}$ are the M-dimensional vectors containing the radii ρ_m and the sampling steps $\Delta\chi_m$, respectively, and σ_r are the Singular Values of $\underline{\underline{T}}$, arranged in a decreasing order.

The Global Optimization of Ψ is obtained using a Differential Evolution approach [11].

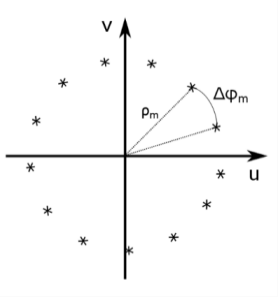

Figure 2. Geometry of the plane-polar grid.

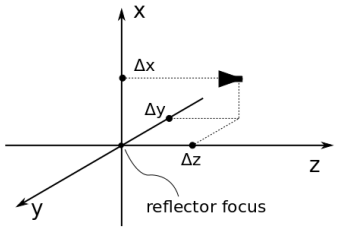

Figure 3. Geometry of the feed displacement.

A. *Feed Position Retrieval*

Once the aberration function is obtained, the feed position is retrieved through a second optimization procedure. Considering a feed displacement from the nominal position $(\Delta x, \Delta y, \Delta z)$, as shown in Figure 3. , the aberration function can be obtained by applying Geometrical Optics (GO). Since we are interested only in the phase perturbation of E_a, the solution of the transport equation is not required, and only the optical path from the feed to the aperture through the reflection must be calculated. In principle, an approach like [12] could be used, but a standard Ray-Tracing algorithm, particularly if optimized [13], is much more efficient, being the medium wherein the AUT is embedded homogeneous. Therefore the displacement $(\Delta x, \Delta y, \Delta z)$ can be found minimizing the functional:

$$\Psi_{GO} = \left\| E_{a0} exp\left(j\Phi_{GO}(x, y, \Delta x, \Delta y, \Delta z)\right) - E_{a0} exp(j\phi) \right\| \quad (7)$$

Where Φ_{GO} is the phase distorsion calculated thanks to GO, as a function of the feed position.

This second optimization step can be straightforwardly obtained by using a gradient-based Local Optimizer.

IV. Numerical Results

In this section some results of a wide numerical analysis are presented. Here we consider a lateral displacement translating a linear aberration, but the procedure can be nonetheless extended to include higher order aberrations. To assess the performances, we compare the results with those obtained using a standard approach, based on a standard uniform Cartesian sampling grid, whose spacing agrees with the Nyquist sampling criterion.

In the worked example, the AUT is an offset parabolic reflector working at 10GHz. The offset angle and the focal length are equal to 23° and 0.5m, respectively. The reflector projects an elliptical aperture with semi-axes equal to 0.423m (~14λ) and 0.384m (~13λ) along the x-axis and y-axis, respectively. The illumination is provided by a linearly polarized feed, with an asymmetric tapering along the x-axis and the y-axis of $-12dB$ and $-16dB$, respectively. To realistically simulate the field radiated by the AUT, the PO solver the commercial software FEKO has been used. The amplitude of E_{a0} is shown in Figure 4. . The introduced misalignment is summarized Table 2.

To represent the effects of the lateral displacement of the feed on E_a, the aberration function has been expressed as:

$$\Phi = p_1 \mathrm{x} + p_2 \mathrm{y} \quad (8)$$

To calculate the PCA, a discretization of $\mathcal{M}$ has been considered by varying the parameters p_1, p_2 in the range $[-5,5] \times [-5,5]$, related to a maximum displacement of 50mm. Thanks to the PCA, an accurate representation of Φ can be obtained by using 19 basis functions.

To make a realistic example, the far-field data has been corrupted by an additive white Gaussian noise with a signal to noise ratio of 30dB. Figure 5. presents the amplitude of the FFP to be sampled.

After the optimization of the SVB of $\underline{\underline{T}}$ a sampling grid of 24 points distributed over 2 rings appears sufficient to make the diagnosis possible. The values of ρ and Δχ are summarized in Table 1.

TABLE I. Parameters of the Optimized Sampling Grid.

Rings	ρ	Δχ
1	0.0434	0.5235
2	0.0724	0.5192

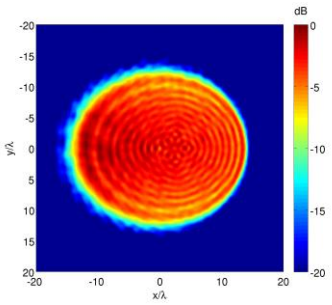

Figure 4. Normalized amplitude in dB of E_{a0}.

For the sake of comparison a standard approach has been implemented. Only the region $[-0.3,0.3] \times [-0.3,0.3]$ of the (u, v) plane has been taken into account, to avoid measurements of useless FFP samples significantly corrupted by the noise. For this second case, the overall number of sampling points is equal to 289.

TABLE II. DISPLACEMENT OF THE FEED.

	Δx [mm]	Δy [mm]
Nominal	0	13.0
Retrieved	0	12.43

Figure 6. and Figure 7. show the amplitude of the reconstructed FFP for the standard grid and the optimized one, respectively. Figure 8. and Figure 9. display a cut along the v-axis, showing that both grids can effectively represent the FFP of the AUT. The Φ retrieved is shown in Figure 10. and Figure 11. for the standard grid and the optimized one, respectively. The displacement of the feed from the reflector focus corresponding to the retrieved Φ is compared to its nominal position in Table 2, showing an error of 0.57mm ($\sim 19 \cdot 10^{-3}\lambda$) in the diagnosis of the position.

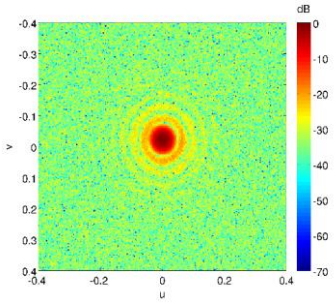

Figure 5. Amplitude (dB) of the simulated FFP corrupted by noise.

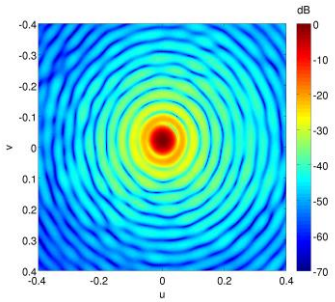

Figure 6. Normalized amplitude (dB) of the reconstructed FFP on the standard grid.

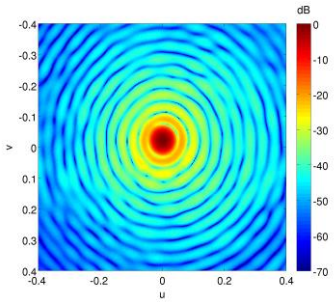

Figure 7. Normalized amplitude (dB) of the reconstructed FFP on the optimized grid.

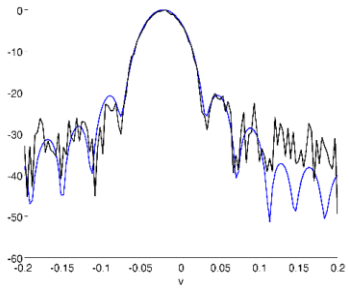

Figure 8. Cut along the v-axis of the normalized amplitude (dB) of the reconstructed FFP on the standard grid. The black line represents the far-field data while the blue line represents the reconstructed field.

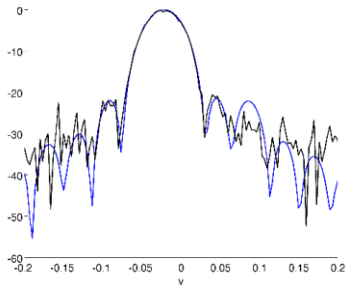

Figure 9. Cut along the v-axis of the normalized amplitude (dB) of the reconstructed FFP on the optimized grid. The black line represents the far-field data while the blue line represents the reconstructed field.

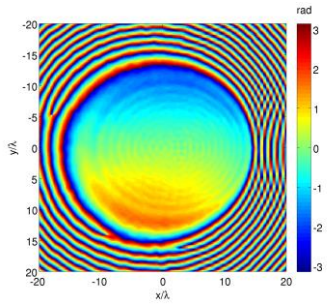

Figure 10. Phase of the aberration function retrieved on the standard grid.

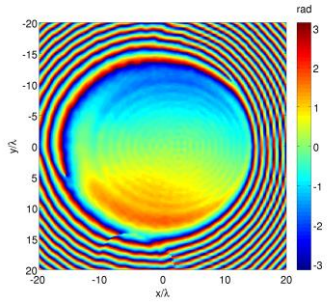

Figure 11. Phase of the aberration function retrieved on the optimized grid.

V. CONCLUSIONS

An efficient diagnosis technique for the diagnosis of feed misalignments in reflector antennas has been presented.

The approach relies on a singular-values optimization procedure to find the number and the location of the far field sampling points required to retrieve the antenna status, allowing a reduction of the measurement time length.

The performances have been numerically tested for a lateral displacement of the feed of an offset parabolic reflector, and compared to a standard sampling acquisition scheme based on the Nyquist criterion, showing that the correct position can be recovered using roughly a tenth of the sampling points.

REFERENCES

[1] Rochblatt, D. J., B. L. Seidel, "Microwave Antenna Holography", IEEE Trans. on Microwave Theory and Techniques, vol. 40, n. 6, June 1992.

[2] Rajagopalan, H., Y. Rahmat-Samii, "Reflector Surface Distortion on a Sub-Reflectarray Cassegrain System: Simulations, Measurements, and Microwave Holographic Diagnostics", Proc. of the Antennas Prop. Society Int. Symp., Chicago, IL, Jul. 8-14, 1-2 (2012).

[3] Baars, J. W. M., R. Lucas, J. G. Mangum and J. A. Lopez-Perez, "Near-Field Radio Holography of Large Reflector Antennas," in IEEE Antennas and Propagation Magazine, vol. 49, no. 5, pp. 24-41, Oct. 2007.

[4] Bolli, P., G. Mazzarella, G. Montisci, and G. Serra, "An alternative solution for the reflector surface retrieval problem," Progress In Electromagnetics Research, Vol. 82, 167-188, 2008.

[5] Capozzoli, A., G. D'Elia, "Global Optimization and Antennas Synthesis and Diagnosis, Part One: Concepts, Tools, Strategies and Performances", Progr. in Electromagn. Res., Volume 56, 195-232 (2006).

[6] Capozzoli, A., G. D'Elia, "Global Optimization and Antennas Synthesis and Diagnosis, Part Two: Applications to Advanced Reflector Antennas Synthesis and Diagnosis Techniques", Progr. in Electromagn. Res., Volume 56, 233-261 (2006).

[7] Nikolic, B., R. M. Prestage, D. S. Balser, C. J. Chandler, and R. E. Hills, "Out-of-focus holography at the Green Bank Telescope", Astronomy & Astrophysics 465, no. 2, 685-693 (2007).

[8] Silver, S., Microwave Antenna Theory and Design, MIT Rad. Lab Series 12, New York, McGraw-Hill, 1949.

[9] Capozzoli, A., C. Curcio, A. Liseno, "NUFFT-Accelerated Plane-Polar (also Phaseless) Near-Field/Far-Field Transformation", Progr. in Electromagn. Res. M., Volume 27, 59-73 (2012).

[10] Capozzoli, A., C. Curcio, A. Liseno, P. Vinetti, "Field Sampling and Field Reconstruction: a New Perspective", Radio Sci., Volume 45, RS6004, 31 pp., 2010, doi:10.1029/2009RS004298.

[11] Storn, R., Price K., "Differential Evolution - A Simple and Efficient Heuristic for Global Optimization over Continuous Spaces", Journal of Global Optimization, 11, 341–359, 1997.

[12] Capozzoli, A., C. Curcio, A. Liseno, and S. Savarese, "GO solutions with Fast Marching.", 2016 10th European Conference on Antennas and Propagation (EuCAP), pp. 1 5. IEEE, 2016.

[13] Breglia, A., A. Capozzoli, C. Curcio, and A. Liseno, "Ultrafast ray tracing for electromagnetics via kD-tree and BVH on GPU.", In Applied Computational Electromagnetics (ACES), 2015 31st International Review of Progress in, pp. 1-2. IEEE, 2015.